mathematics

MDPI

Article

Nonconvex Tensor Relative Total Variation for Image Completion

Yunqing Bai [1], Jihong Pei [1] and Min Li [2,*]

[1] ATR National Key Laboratory of Defense Technology, Shenzhen University, Shenzhen 518060, China
[2] College of Mathematics and Statistics, Shenzhen University, Shenzhen 518060, China
* Correspondence: limin800@szu.edu.cn

Abstract: Image completion, which falls to a special type of inverse problems, is an important but challenging task. The difficulties lie in that (i) the datasets usually appear to be multi-dimensional; (ii) the unavailable or corrupted data entries are randomly distributed. Recently, low-rank priors have gained importance in matrix completion problems and signal separation; however, due to the complexity of multi-dimensional data, using a low-rank prior by itself is often insufficient to achieve desirable completion, which requires a more comprehensive approach. In this paper, different from current available approaches, we develop a new approach, called relative total variation (TRTV), under the tensor framework, to effectively integrate the local and global image information for data processing. Based on our proposed framework, a completion model embedded with TRTV and tensor p-shrinkage nuclear norm minimization with suitable regularization is established. An alternating direction method of multiplier (ADMM)-based algorithm under our framework is presented. Extensive experiments in terms of denoising and completion tasks demonstrate our proposed method are not only effective but also superior to existing approaches in the literature.

Keywords: tensor completion; tensor relative total variation; tensor p-shrinkage nuclear norm

MSC: 68U10; 94A08

check for updates

Citation: Bai, Y.; Pei, J.; Li, M. Nonconvex Tensor Relative Total Variation for Image Completion. *Mathematics* **2023**, *11*, 1682. https://doi.org/10.3390/math11071682

Academic Editors: Yiu-ming Cheung, Yuping Wang and Xin Liu

Received: 28 February 2023
Revised: 23 March 2023
Accepted: 29 March 2023
Published: 31 March 2023

Copyright: © 2023 by the authors. Licensee MDPI, Basel, Switzerland. This article is an open access article distributed under the terms and conditions of the Creative Commons Attribution (CC BY) license (https://creativecommons.org/licenses/by/4.0/).

1. Introduction

Data missing often occurs in various applications and is the one of the most common problems appeared in information acquisition, requiring the recovery of those missing ones, which consequently leads to the study of completion problems. More specifically, a completion task aims to estimate the missing (or corrupted) entries of an image by leveraging the inherent structural prior as well as available reference information. Practically, the effectiveness of completion is critical in many applications, such as in computer vision and biomedical engineering, in which detection, classification, and recognition are required. Hence, it is not only important but also necessary to develop effective models with efficient processes to achieve desirable image completions.

Since image data are usually obtained by multi-spectral measures or microphone arrays expressed as linear combinations of a few patterns, low-rank property holds naturally for data [1]. During the past decade, many low-rank-based approaches for completion have been proposed. For instance, the low-rank matrix completion (LRMC) adopted the convex relaxation of rank to construct the corresponding approximation [2–4]. However, nowadays, real data collected in many application areas are usually expressed as multi-way arrays, which are tensors. On the other hand, how to generalize the properties satisfied by matrix modeling to tensors is also a task worthy of further exploration.Therefore, low-rank tensor completion (LRTC) has been a hot topic in computer vision [5–8]. For LRTC, the definition of tensor rank is not unique. For example, Kruskal introduced decomposition of CANDECOMP/RARAFAC (CP) rank and Tucker rank for tensor [9–12].

Zhang et al. provided a tubal rank based on tensor-Singular Value Decomposition (t-SVD) for completion of multi-linear data [13]. As an extension of the above model, Zhang et al. continued to use this tubal rank to explore the problem of completion for panning video sequences under random sampling of the data cube, which can be summarized as multi-rank or average rank [14]. Owing to the nonconvexity and nonsmoothness of these rank functions, the corresponding models are hard to solve. Therefore, a large number of convex relaxation optimization strategies for rank functions of tensors are presented, where it is popular to approximate the low-rank tensor using the corresponding convex envelope (i.e., tensor nuclear norm).

It is well known that the tensor nuclear norm has different forms due to the diversity of the rank definition. For example, by means of CP decomposition, rank function can be relaxed as CP tensor nuclear norm (CNN) [15]. For Tucker decomposition, Liu et al. proposed to use the sum of nuclear norm with mode-i expansion (SNN) instead of a Tucker rank [7]. However, these presentations always destroy the internal structure of data, and thus, Zhang et al. proposed another tensor nuclear norm (TNN) which is based on the sum of singular values from all positive slices of the tensor in the Fourier domain [13]. Using t-SVD, Lu et al. showed that TNN can be expressed as a convex envelope of an average rank tensor under certain constraints [16]. However, the disadvantage of the above relaxations is the existence of a gap between the rank function and nuclear norm, which causes solution deviation.

To address this disadvantage, nonconvex low-rank tensor approximation has received significant attention in recent years. For instance, the nonconvex surrogate based on Laplace function is explored for low-rank tensors, which can adaptively assign weights to different singular values [17] to prevent over-punishment of large singular values. The nonconvex Schatten-p ($0 < p < 1$) quasi-norm is known theoretically to manipulate at least as well for recovering low-rank matrices from limited measurements [18–26]. To treat all singular values differently, Liu et al. proposed the tensor p-shrinking nuclear norm based on T-SVD [27], which is very competitive in completion.

Inspired by these works, we attempt to introduce an image completion model, including the nonconvex tensor p-shrinkage norm and tensor-based relative total variation (TRTV) in this paper. Compared to TNN-based models [1,28,29], tensor p-shrinkage norm has potentiality in the approximation for low-rank tensor. Furthermore, TRTV can capture overall spatial variations of image and remove the noise. Additionally, the algorithm based on the framework of alternating direction multiplier method (ADMM) for this model is provided. Moreover, we compare the proposed method with other state-of-the-art algorithms by considering several types of noise on the missing data, e.g., Gaussian noise with different variances, salt & pepper noise, multiplicative speckle noise, and many others.

The remainder of this paper is organized as follows: Section 2 provides a preliminary introduction as well as some recent related works. The proposed model and the corresponding algorithm are illustrated in Section 3. Extensive experiment results are provided in Section 4. The paper ends with concluding remarks in Section 5.

2. Notation and Background

In this section, the main notations and definitions used later are introduced. Simultaneously, we provide the regular terms that are related to the proposed method.

2.1. Tensor-Based Notations

For a given three-order tensor $\mathcal{X} \in \mathbb{R}^{n_1 \times n_2 \times n_3}$ ($\mathbb{R}$ is the field of real numbers), $\mathbf{X}_{(k)}$ is the k-th frontal slice. $\mathcal{X}_{i,j,k}$ is the (i,j,k)-th element of this tensor. $\circ$ is the Hadamard product, which is a multiplication operation on the elements at corresponding positions. $\langle \cdot, \cdot \rangle$ is the inner product of two tensors, which can be expressed as $\langle \mathcal{X}, \mathcal{Y} \rangle = \sum_{i,j,k} \mathcal{X}_{i,j,k} \mathcal{Y}_{i,j,k}$. The Frobenius norm is defined as $\|\mathcal{X}\|_F = \sqrt{\langle \mathcal{X}, \mathcal{X} \rangle}$. $\mathcal{X}^T$ is the transpose tensor.

Let L be an invertible linear transform (such as wavelet transform or Fourier transform), while $\bar{\mathcal{X}}$ is denoted as a result of $\mathcal{X}$ under L, i.e., $\bar{\mathcal{X}} = L(\mathcal{X})$. The block circulant matrix of $\mathcal{X}$ [27,30] is defined as:

$$bcirc(\mathcal{X}) = \begin{bmatrix} \mathbf{X}_{(1)} & \mathbf{X}_{(n_3)} & \cdots & \mathbf{X}_{(2)} \\ \mathbf{X}_{(2)} & \mathbf{X}_{(1)} & \cdots & \mathbf{X}_{(3)} \\ \vdots & \vdots & \ddots & \vdots \\ \mathbf{X}_{(n_3)} & \mathbf{X}_{(n_3-1)} & \cdots & \mathbf{X}_{(1)} \end{bmatrix}. \tag{1}$$

The unfold operator and its inverse manipulation can be expressed as:

$$unfold(\mathcal{X}) = \begin{bmatrix} \mathbf{X}_{(1)} \\ \mathbf{X}_{(2)} \\ \vdots \\ \mathbf{X}_{(n_3)} \end{bmatrix} \in \mathbb{R}^{n_1 n_3 \times n_2}, \tag{2}$$

$$fold(unfold)(\mathcal{X})) = \mathcal{X}. \tag{3}$$

Next, we give some important results used in this paper.

Definition 1 (T-product [31]). *For tensors $\mathcal{A} \in \mathbb{R}^{n_1 \times n_2 \times n_3}$ and $\mathcal{B} \in \mathbb{R}^{n_2 \times n_4 \times n_3}$, the T-product of $\mathcal{A}$ and $\mathcal{B}$ under invertible linear L, is defined as:*

$$\mathcal{C} = \mathcal{A} *_L \mathcal{B} \in \mathbb{R}^{n_1 \times n_4 \times n_3}. \tag{4}$$

Definition 2 (T-SVD [31]). *For a given tensor $\mathcal{X} \in R^{n_1 \times n_2 \times n3}$, then it can be factored as:*

$$\mathcal{X} = \mathcal{U} *_L \mathcal{S} *_L \mathcal{V}^*, \tag{5}$$

where $\mathcal{S} \in R^{n_1 \times n_2 \times n3}$ is a f-diagonal tensor, $\mathcal{U} \in R^{n_1 \times n_1 \times n3}$ and $\mathcal{V} \in R^{n_2 \times n_2 \times n3}$ are orthogonal tensors,i.e., $\mathcal{U}^T * \mathcal{U} = \mathcal{U} * \mathcal{U}^T = I$, $\mathcal{V}^T * \mathcal{V} = \mathcal{V} * \mathcal{V}^T = I$.

Particularly, if L is discrete Fourier transformation of tensor along the third dimension, we have $\bar{\mathcal{X}} = fft(\mathcal{X}, [], 3)$ (fft is an expression from MATLAB). The corresponding inverse operation is $\mathcal{X} = ifft(\bar{\mathcal{X}}, [], 3)$, and the t-product is expressed as $\mathcal{C} = fold(bcric(\mathcal{A})) \cdot unfold(\mathcal{B})$. Now, T-SVD actually performs the Fourier transform of the tensor first, and then gives the SVD decomposition of the matrix for each frontal slice of the tensor.

2.2. Related Low-Rank Models

It is well known that the LRTC aims at extracting the low-rank and clean N-th order tensor $\mathcal{X}$ from input tensor $\mathcal{T}$ without noise. Mathematically, this problem can be formulated as [13]:

$$\begin{aligned} &\min_{\mathcal{X}} rank(\mathcal{X}) = \frac{1}{n_3} \sum_{k=1}^{n_3} \text{rank}\left(\bar{\mathbf{X}}_{(i)}\right) \\ &\text{s.t.} P_\Omega(\mathcal{X}) = P_\Omega(\mathcal{T}), \end{aligned} \tag{6}$$

where $\mathcal{T}, \mathcal{X} \in \mathbb{R}^{n_1 \times n_2 \times \cdots \times n_N}$, $\Omega = \{(i_1, i_2, \ldots, i_N) | \mathcal{T}_{i_1, i_2, \ldots, i_N} \text{ is observed}\}$ is a support set. The missing operation of data is illustrated by an index function P_Ω, i.e.:

$$P_\Omega(\mathcal{T}_{i_1, i_2, \ldots, i_N}) = \begin{cases} \mathcal{T}_{i_1, i_2, \ldots, i_N}, & if \quad i_1, i_2, \ldots, i_N \in \Omega, \\ 0, & \text{otherwise.} \end{cases} \tag{7}$$

Due to the discrete nature of the rank, the solution of Equation (6) is NP-hard and intractable. A common approach is to use the convex relaxation replacing the rank function.

In detail, for a given tensor, the tensor average rank actually calculates the average number of nonzero singular values of all frontal slices in the Fourier transform domain. Thus, the nuclear norm associated with singular values is defined as in Equation (8), which is the convex approximation for the tensor average rank (TNN):

$$\|\mathcal{X}\|_{TNN} = \sum_{i=1}^{N} \left\| \bar{\mathbf{X}}_{(i)} \right\|_*, \tag{8}$$

where $\bar{\mathbf{X}}_i \in R^{n_i \times \prod_{k \neq i} n_k}$ is i-th frontal slice of the tensor $\bar{\mathcal{X}}$ under invertible linear transform. The nuclear norm $\|\cdot\|_*$ is the sum of singular values. Hereupon, problem Equation (6) can be rewritten as:

$$\min_{\mathcal{X}} \|\mathcal{X}\|_{TNN} \ \text{s.t.} P_\Omega(\mathcal{X}) = P_\Omega(\mathcal{T}). \tag{9}$$

To alleviate the deficiency of the convex relaxation in Equation (9), we propose to use the tensor p-shrinkage nuclear norm(p-TNN) to approach rank. Specifically, the definition of p-TNN is as follows:

Definition 3 ([27]). *Let $\mathcal{Z} \in \mathbb{R}^{n_1 \times n_2 \times n_3}$, $\forall \mu > 0$, $p \leq 1$ and its t-SVD be $\mathcal{Z} = \mathcal{U} *_L \mathcal{S} *_L \mathcal{V}^*$, so p-TNN can be written as:*

$$\|\mathcal{Z}\|_p = \frac{1}{n_3} \sum_{i=1}^{n_3} \left\| \bar{\mathbf{Z}}_{(i)} \right\|_p \tag{10}$$

$$= \frac{1}{n_3} \sum_{k=1}^{n_3} \sum_{i=1}^{\min\{n_1, n_2\}} S_p^\mu(\bar{\mathcal{S}}), \tag{11}$$

where $s_p^\mu(\bar{\mathcal{S}}_{iik}) = sign(\bar{\mathcal{S}}_{iik}) max(|\bar{\mathcal{S}}_{iik}| - \mu |\bar{\mathcal{S}}_{iik}|^{p-1}, 0)$, $\bar{\mathcal{S}}_{iik}$ is the (i,i,k)-th tensor singular value of $\bar{\mathcal{Z}}$, and L is DFT.

It is easy to prove that p-TNN satisfies the properties defined in [27], such as positivity, nonconvexness, unitary invariance, and tightness. Among them, tightness indicates that p-TNN is a tighter envelope within the unit ball of the spectral norm. This also demonstrates that p-TNN is a better approximation of rank, which can give a better solution. In fact, s_p^μ in Equation (11) is the p-shrinkage thresholding operator, whose definition is:

Definition 4 ([32]). *Let any $x \in \mathbf{R}$, $\forall \mu > 0$, $p \leq 1$, the p-shrinkage thresholding operator s_p^μ. It can be expressed in the following form:*

$$s_p^\mu(x) = sign(x) max\{|x| - \mu |x|^{p-1}, 0\}. \tag{12}$$

Figure 1 shows the effect of some function terms on the singular value x of each frontal slice in the Fourier transform domain, which includes the tensor average rank, while TNN and p-TNN values are taken p as negative infinity, $-\frac{1}{2}$, $\frac{1}{2}$, respectively. If set $p = 1$, the Equation (12) can be written as $s_p^\mu(\bar{\mathcal{S}}_{iik}) = max(|\bar{\mathcal{S}}_{iik}| - \mu, 0)$, which is equivalent to the soft threshold operator of a singular value. When $p \to -\infty$, Equation (11) is a hard threshold without penalty for large inputs. However, setting $p = -\frac{1}{2}, \frac{1}{2}$, Equation (12) usually penalizes less for the larger input.

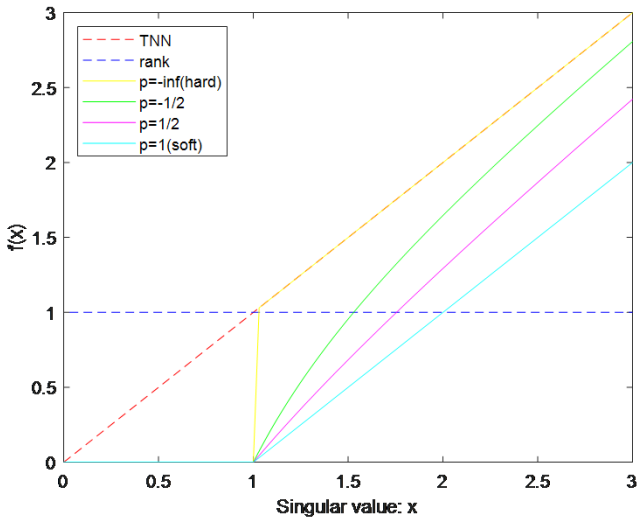


Figure 1. Approximation of rank from p-TNN, TNN, and tensor average rank acting on the frontal slice, respectively, where the x-axis is the singular value, while the y-axis denotes the results obtained by p-TNN, TNN, and tensor average rank.

2.3. Tensor Relative Total Variation

Generally, smoothness is an important property of real data. Yokota et al. [29] employed PARAFAC/Polyadic decomposition (PD) based on the total variation (TV) and quadratic variation (QV) to achieve tensor completion. In addition, the newly defined TV is used to embody the advantages of the smoothness constraint in [1,28]. Since TV can preserve edges and eliminates noise in flat areas, it shows superiority in dealing with various types of image recovery tasks [8,33–35].

On the other hand, the organic spatial spectral total variation (SSTV) regularization is given, which can capture the piecewise smooth structure in both spatial domain and spectral domain for hyperspectral images (HSIS) [36]. In fact, SSTV is a 3D weighted extended version of TV. However, SSTV does not capture the overall spatial variation. Thus, the windowed total variations (WTV) is proposed [37], which can be denoted as:

$$\mathscr{D}_x(p_0) + \mathscr{D}_y(p_0) = \sum_{q \in R(p_0)} w_{p_0,q} \left| (\partial_x Y)_q + (\partial_y Y)_q \right|, \tag{13}$$

where $\mathscr{D}_x(p_0)$ and $\mathscr{D}_y(p_0)$ are windowed total variations in the x and y direction for pixel p_0. Y is the given image. $q \in R(p_0)$ means the element of the rectangular region centered at pixel p_0. $w_{p_0,q}$ is the weight of $\mathscr{D}$ based on spatial affinity, which can be written as:

$$w_{p_0,q} = \exp\left(-\frac{(x_{p_0} - x_q)^2 + (y_{p_0} - y_q)^2}{2\sigma^2} \right), \tag{14}$$

where σ is used to control the spatial scale of the window. $\mathscr{D}$ is the sum of the weighted total variations in the region $R(p_0)$ centered on the pixel p_0.

However, this metric is defined based on local gradients in different directions, which can also produce a step effect or transition smoothing in the image smooth area with noise. For example, it is a consensus that the unwanted textures of an image is a kind of noise for image structure. Thus, WTV is not good at distinguishing noise from texture structure. To address this problem, the relative total variation (RTV) is proposed to capture the main structure and remove noise simultaneously [37]. Therefore, the corresponding formulation is as follows:

$$G_{RTV}(Y) = \sum_{p_0}\left(\frac{\mathscr{D}_x(p_0)}{\mathscr{L}_x(p_0)+\varepsilon} + \frac{\mathscr{D}_y(p_0)}{\mathscr{L}_y(p_0)+\varepsilon}\right), \tag{15}$$

$$\mathscr{L}_x(p_0) = \left|\sum_{q\in R(p_0)} w_{p_0,q}\cdot(\partial_x Y)_q\right|, \tag{16}$$

$$\mathscr{L}_y(p_0) = \left|\sum_{q\in R(p_0)} w_{p_0,q}\cdot(\partial_y Y)_q\right|, \tag{17}$$

where ε is a small parameter, which is used to make the calculation meaningful and prevent zero as denominator, $\mathscr{L}_x(p_0)$ and $\mathscr{L}_y(p_0)$ are the windowed inherent variation (WIV) in different directions, and $w_{p_0,q}$ is the weight between pixels p_0 and q. RTV is better able to capture some internal change, since the partial derivatives in different direction $\partial_x Y$ or $\partial_y Y$ may be negative. Motivated by previous studies, we designed tensor relative total variation (TRTV), which is incorporated into the smooth and low-rank constraint framework. Since the structural characteristics of each front slice are specific to their own features, RTV is used for each front slice of the tensor according to the characteristics of total change and internal change. Hence, we have the following:

Definition 5. *For tensor $\mathcal{Y} \in \mathbb{R}^{n_1\times n_2\times n_3}$, the tensor relative total variation(TRTV) can be expressed as*

$$f_{TRTV}(\mathcal{Y}) = \sum_{k=1}^{n_3} G_{RTV}(\mathcal{Y}(:,:,k)). \tag{18}$$

3. The Proposed Model

By and large, the simultaneous tensor completion and denoising problem is usually expressed as:

$$\begin{aligned} \min_{\mathcal{X}} \ & \alpha\phi(\mathcal{X}) + \beta f_{LR}(\mathcal{X}) \\ \text{s.t.} & \|P_\Omega(\mathcal{T}-\mathcal{X})\|_F^2 \le \delta \\ & \mathcal{X} \in [v_{\min}, v_{\max}]. \end{aligned} \tag{19}$$

where $\mathcal{T}$ and $\mathcal{X}$ are, respectively, the input and output N-th order tensors, $f_{LR}(\cdot)$ is the low-rank regularization, $\phi(\cdot)$ evaluates smoothness, $P_\Omega(\cdot)$ is an index tensor which denotes the missing and available elements of $\mathcal{T}$ as 1 and 0, δ is the noise level of the observed elements in $\mathcal{T}$, $[v_{\min}, v_{\max}]$ means the numerical range of the output tensor $\mathcal{X}$, and $\alpha \in [0,1]$ and $\beta = 1-\alpha$ are parameters which balance the first and second items.

In [1,28,29], $f_{LR}(\cdot)$ is characterized by TNN, while $\phi(\cdot)$ considers, respectively, total variation (TV) and quadratic variation (QV). Different from previous studies, we propose to use p-TNN for the low-rank and tensor relative total variation (TRTV) regularizer as a smooth operator. Thus, Equation (19) can be written as:

$$\begin{aligned} \min_{\mathcal{X}} \ & \alpha f_{\mathrm{TRTV}}(\mathcal{X}) + \beta\|\mathcal{X}\|_p \\ \text{s.t.} \ & \|P_\Omega(\mathcal{T}-\mathcal{X})\|_F^2 \le \delta \\ & \mathcal{X} \in [v_{\min}, v_{\max}]. \end{aligned} \tag{20}$$

It is easy to find that the two constraints in Equation (20) can be converted to the following indicator functions i_δ and i_D, i.e.,:

$$\begin{aligned} i_{\mathcal{D}}(\mathcal{X}) &:= \begin{cases} 0 & v_{\min} \le \mathcal{X} \le v_{\max}, \\ \infty & \text{otherwise}. \end{cases} \\ i_\delta(\mathcal{X}) &:= \begin{cases} 0 & \|P_\Omega(\mathcal{T}-\mathcal{X})\|_F^2 \le \delta, \\ \infty & \text{otherwise}. \end{cases} \end{aligned} \tag{21}$$

Therefore, by integrating Equations (20) and (21), the new model can be rewritten as:

$$\underset{\mathcal{X}}{\text{minimize}} \quad i_\delta(\mathcal{X}) + i_D(\mathcal{X}) + \alpha f_{TRTV}(\mathcal{X}) + \beta\|\mathcal{X}\|_p. \tag{22}$$

Optimization

In Section 2, the properties of p-TNN and TRTV are introduced. Note that the singularity threshold is determined by μ and p. A larger singular threshold results in excessive loss of nonnoise-induced information. It is easy to find that $f_{TRTV}(\mathcal{X})$ and $\|\mathcal{X}\|_p$ are correlated, since both deal with the same tensor. Furthermore, the objective function (22) involves the local segment smooth term and global low rank for the restored image.

To solve problem (22) more conveniently, we introduce the auxiliary variables $\mathcal{N}$, $\mathcal{Y}$ and $\mathcal{Z}$. Thus, the minimization of Equation (22) is equivalent to:

$$\begin{array}{ll} \min\limits_{\mathcal{X}} & i_\delta(\mathcal{X}) + i_D(\mathcal{N}) + \alpha f_{TRTV}(\mathcal{Y}) + \beta\|\mathcal{Z}\|_p \\ \text{s.t.} & \mathcal{N} = \mathcal{Y}, \mathcal{Z} = \mathcal{Y}, \mathcal{Y} = \mathcal{X}. \end{array} \tag{23}$$

The corresponding augmented Lagrangian function of Equation (23) is as follows:

$$\begin{array}{l} \mathcal{L}(\mathcal{X}, \mathcal{N}, \mathcal{Z}, \mathcal{Y}, \mathcal{T}_1, \mathcal{T}_2, \mathcal{T}_3,) \\ = i_\delta(\mathcal{X}) + i_D(\mathcal{N}) + \alpha \sum_{k=1}^{n_3} G_{RTV}(\mathcal{Y}(:,:,k)) + \beta\|\mathcal{Z}\|_p \\ + \langle \mathcal{T}_1, \mathcal{N} - \mathcal{Y}\rangle + \langle \mathcal{T}_2, \mathcal{Z} - \mathcal{Y}\rangle + \langle \mathcal{T}_3, \mathcal{Y} - \mathcal{X}\rangle \\ + \frac{\mu}{2}(\|\mathcal{N} - \mathcal{Y}\|_F^2 + \|\mathcal{Z} - \mathcal{Y}\|_F^2 + \|\mathcal{Y} - \mathcal{X}\|_F^2). \end{array} \tag{24}$$

where $\mathcal{T}_i, i = 1, 2, 3$ are Lagrange multiplier tensors and μ is the penalty parameter for the augmentation term.

Due to the separation of variables, we utilize the alternating direction multiplier method (ADMM) to solve Equation (24).

- Update $\mathcal{X}$

  To extract all terms related to $\mathcal{X}$ from the augmented Lagrangian function (24), we need to solve the following subproblem:

$$\begin{aligned} &\min_{\mathcal{X}} i_\delta(\mathcal{X}) + \langle \mathcal{T}_3, \mathcal{Y} - \mathcal{X}\rangle + \tfrac{\mu}{2}\|\mathcal{Y} - \mathcal{X}\|_F^2 \\ &= \min_{\mathcal{X}} i_\delta(\mathcal{X}) + \tfrac{\mu}{2}\left\|\mathcal{X} - \mathcal{Y} + \tfrac{\mathcal{T}_3}{\mu}\right\|_F^2 \end{aligned} \tag{25}$$

  Set $D_\Omega(\mathcal{X}, \mathcal{T}) = \|P_\Omega(\mathcal{X}) - P_\Omega(\mathcal{T})\|_F^2$; the proximal function of $i_\delta(\cdot)$ problem is given as follows:

$$\min_{\mathcal{X}} \frac{1}{2}\|\mathcal{X} - \mathcal{H}\|_F^2 + i_\delta(\mathcal{X}). \tag{26}$$

  Equation (26) is equivalent to the following problem:

$$\min_{\mathcal{X}} \frac{1}{2}\|\mathcal{X} - \mathcal{H}\|_F^2, s.t. \|\mathcal{Q} \circ (\mathcal{X} - \mathcal{T})\|_F^2 \leq \delta, \tag{27}$$

  where $\mathcal{H}$ is the arbitrary variables and $\circ$ can be the Hadamard product. The optimal value can be given as follows [1,28]:

$$\begin{array}{l} prox_{i_\delta}(\mathcal{H}) = \mathcal{Q}_1 \circ \mathcal{T} + (1 - \mathcal{Q}_1) \circ \mathcal{H}, \\ \mathcal{Q}_1 = max(0, 1 - \frac{\sqrt{\delta}}{\|\mathcal{Q} \circ (\mathcal{H} - \mathcal{T})\|_F})\mathcal{Q}. \end{array} \tag{28}$$

  Therefore, the minimization of Equation (25) can be denoted as:

$$\mathcal{X} = prox_{i_\delta}(\mathcal{Y} - \tfrac{\mathcal{T}_3}{\mu}). \tag{29}$$

- Update $\mathcal{N}$
  Let other variable be fixed, $\mathcal{N}$ can be update by solving the following subproblem:

$$\min_{\mathcal{N}} i_D(\mathcal{N}) + \frac{\mu}{2}\left\|\mathcal{N} - \mathcal{Y} + \mu^{-1}\mathcal{T}_1\right\|_F^2. \tag{30}$$

  The closed-form solution is easily obtained by proximal function $prox_{i_D}$:

$$\mathcal{N} = prox_{i_D}(\mathcal{Y} - \mu^{-1}\mathcal{T}_1). \tag{31}$$

- Update $\mathcal{Z}$
  By fixing other variables, updated $\mathcal{Z}$ can be obtained by the following subproblem.

$$\mathcal{Z}^{k+1} = arg\min_{\mathcal{Z}} \beta\|\mathcal{Z}\|_p + \tfrac{\mu}{2}\left\|\mathcal{Z} - \mathcal{Y} + \mu^{-1}\mathcal{T}_2\right\|_F^2. \tag{32}$$

  Set $\mathcal{Z}_0 = \mathcal{Y} - \mu^{-1}\mathcal{T}_2$; the above problem is equivalent to the following subproblem:

$$\min_{\mathcal{Z}} \frac{1}{2}\|\mathcal{Z} - \mathcal{Z}_0\|_F^2 + \tau\|\mathcal{Z}\|_p. \tag{33}$$

  where $\tau = \mu^{-1}\beta$. Inspired by Definition 3 given in Section 2.2, the solution of subproblem (32) can be given by tensor generalized singular value thresholding, i.e.:

  Definition 6. *Tensor generalized singular value thresholding, t-GSVT. For $\forall\tau > 0$ and a given tensor $\mathcal{Z}_0 \in \mathbb{R}^{n_1\times n_2\times n_3}$. Then, a closed-form solution of problem (33) is given by:*

$$prox_{\tau\|\mathcal{Z}\|_p}(\mathcal{Z}_0) = \mathcal{U} * \mathcal{D} * \mathcal{V}^T. \tag{34}$$

  where $\mathcal{S} \in \mathbb{R}^{n_1\times n_2\times n_3}$ is the f-diagonal tensor, and orthogonal tensors $\mathcal{U} \in \mathbb{C}^{n_1\times n_1\times n_3}$ and $\mathcal{V} \in \mathbb{C}^{n_2\times n_2\times n_3}$ are both related to the t-SVD, i.e., $\mathcal{Z}_0 = \mathcal{U} * \mathcal{S} * \mathcal{V}^T$. $\mathcal{D} \in \mathbb{R}^{n_1\times n_2\times n_3}$ is the f-diagonal tensor and satisfies $\overline{D}_{iik} = s_p^{\mu}(\overline{\mathcal{S}}_{iik})$. $\overline{\mathcal{S}}_{iik}$ is the (i,i,k)-th tensor sigular value of $\overline{\mathcal{S}}$.

  Specifically, the minimization of Equation (32) can be summarized as:

$$\mathcal{Z} = prox_{\beta\|\mathcal{Z}\|_p}(\mathcal{Y} - \mu^{-1}\mathcal{T}_2). \tag{35}$$

- Update $\mathcal{Y}$
  By fixing $\mathcal{X}^{k+1}, \mathcal{N}^{k+1}, \mathcal{Z}^{k+1}, \mathcal{T}_i^k, i = 1,2,3$, we can obtain $\mathcal{Y}$ by the following subproblem:

$$\begin{aligned}\min_{\mathcal{Y}} \sum_{k=1}^{n_3} G_{RTV}(\mathcal{Y}(:,:,k)) + \frac{\mu}{2}\left\|\mathcal{N} - \mathcal{Y} + \mu^{-1}\mathcal{T}_1\right\|_F^2 \\ + \frac{\mu}{2}\left\|\mathcal{Z} - \mathcal{Y} + \mu^{-1}\mathcal{T}_2\right\|_F^2 + \frac{\mu}{2}\left\|\mathcal{Y} - \mathcal{X} + \mu^{-1}\mathcal{T}_3\right\|_F^2.\end{aligned} \tag{36}$$

  Equation (36) can be written as the following equivalent form:

$$\min_{\mathcal{Y}} f_{TRTV}(\mathcal{Y}) + \frac{\mu}{2}\|\mathcal{Y} - \mathcal{Y}'\|_F^2, \tag{37}$$

  where $\mathcal{Y}' = \frac{1}{3}(\mathcal{N} + \mathcal{Z} + \mathcal{X} + \mu^{-1}(\mathcal{T}_1 + \mathcal{T}_2 - \mathcal{T}_3))$. TRTV term can deal with inhomogeneous and anisotropic texture better. In detail, for the k-th frontal section of $\mathcal{Y}$ and $\mathcal{Y}'$, the corresponding optimized problem is as follows:

$$\min_{\mathbf{Y}_{(k)}} \frac{\mu}{2}\left\|\mathbf{Y}_{(k)} - \mathbf{Y}'_{(k)}\right\|_F^2 + G_{RTV}(Y_{(k)}). \tag{38}$$

However, Equation (38) is nonconvex, which results in the diffent optimization. Inspired by RTV on matrix [37], Equation (38) is solvable by vectorizing it into linear problems in each iteration. In detail, set $v_s = vec(\mathcal{Y}(:,:,k))$ and $v_I = vec(\mathcal{Y}'(:,:,k))$. v_s^{t+1} can be obtained by using $(\mathbf{1} + \lambda L^t) \cdot v_s^{t+1} = v_I$, where $\mathbf{1}$ is identity, L^t is a symmetric matrix related to vector v_s^t, and $(\mathbf{1} + \lambda L^t)$ is a Laplacian matrix.

- Update Lagrange multipliers $\mathcal{T}_i, i = 1,2,3$
  After updating $\mathcal{X}^{k+1}$, $\mathcal{N}^{k+1}$, $\mathcal{Z}^{k+1}$, $\mathcal{Y}^{k+1}$, the Lagrange multipliers $\mathcal{T}_i, i = 1,2,3$ are update, respectively, by:

$$\begin{aligned} \mathcal{T}_1 &= \mathcal{T}_1 + \mu(\mathcal{N} - \mathcal{Y}), \\ \mathcal{T}_2 &= \mathcal{T}_2 + \mu(\mathcal{Z} - \mathcal{Y}), \\ \mathcal{T}_3 &= \mathcal{T}_3 + \mu(\mathcal{Y} - \mathcal{X}). \end{aligned} \tag{39}$$

In particular, replacing $\|\cdot\|_p$ by TNN in Equation (20), the corresponding problem can be denoted as:

$$\begin{aligned} \min_{\mathcal{X}} \ & \alpha f_{\mathrm{TRTV}}(\mathcal{X}) + \beta \|\mathcal{X}\|_{TNN} \\ \text{s.t.} \ & \|P_\Omega(\mathcal{T} - \mathcal{X})\|_F^2 \le \delta \\ & \mathcal{X} \in [v_{\min}, v_{\max}]. \end{aligned} \tag{40}$$

The optimization process of Equation (40) is different only for updating the variable $\mathcal{Z}$; the other steps are the same. In this case, the updating of $\mathcal{Z}$ can be denoted as the closed solution by tensor singular value thresholding (T-SVT) operation [16], i.e.:

$$\mathcal{Z}^{k+1} = arg \min_{\mathcal{Z}} \tfrac{\beta}{\mu n_3} \|\mathcal{Z}\|_* + \tfrac{1}{2} \left\|\mathcal{Z} - \mathcal{Y} + \mu^{-1}\mathcal{T}_2\right\|_F^2. \tag{41}$$

In summary, the solving of minimization (23) is expressed as Algorithm 1.

Algorithm 1 Solving problem (23).

Input: the observed tensor data $\mathcal{T}, \Omega, p, \delta, \eta, v_{min}, v_{max}, \mu$
$\alpha, \beta, \mu_{max}, \rho, \epsilon_1, \epsilon_2$
Initialize: $\mathcal{T}_i^0, (i = 1,2,3)$, $\mathcal{X}^0$, $\mathcal{N}^0$, $\mathcal{Y}^0$, $\mathcal{Z}^0$, $k = 0$
While not converge do
1. Update $\mathcal{X}^k$ by solving Equation (28)
2. Update $\mathcal{N}^k$ by solving Equation (31)
3. Update $\mathcal{Z}^k$ by solving Equation (32)
4. Update $\mathcal{Y}^k$ by solving Equation (36)
5. Update $\mathcal{T}_i^k, i = 1,2,3$ by solving Equation (39)
6. $\mu \leftarrow min\{\rho\mu, \mu_{max}\}$
7. Check the convergence condition $\left\|\mathcal{X}^k - \mathcal{X}^{k-1}\right\|_F \le \epsilon_2$ and $\alpha f_{TRTV}(\mathcal{Y}) + \beta\|\mathcal{Z}\|_p \le \epsilon_2$
8. $k \leftarrow k + 1$
end while
Output: $\mathcal{X}^*$

4. Experiments

4.1. Image Pre-Processing and Evaluation Metrics

As we know, gray image can be expressed as a two-order tensor and color image is denoted as a three-order tensor according to row, column, and RGB channel. In this section, we apply the proposed model and the related methods to some color images (as shown in Figure 2).



Figure 2. Description of the standard test images.

Peak Signal to Noise Ratio (PSNR) and Structural similarity index (SSIM) are used to compare our method with state-of-the-art methods. For gray images, PSNR is defined as:

$$PSNR = 10log_{10}\left(\frac{n_1 n_2 \|\mathcal{X}\|_\infty^2}{MSE}\right), \tag{42}$$

where the mean squared error (MSE) is $\|\mathcal{X} - \mathcal{X}^*\|_F$. For tensor PSNR, it is obtained by averaging the PSNR of each channel matrix. The larger its value, the smaller the distortion. For a tensor $\mathcal{X} \in \mathbb{R}^{n_1 \times n_2 \times n_3}$ and an output tensor $\mathcal{X}^* \in \mathbb{R}^{n_1 \times n_2 \times n_3}$, SSIM can be represented as:

$$SSIM = \frac{(2\mu_X \mu_{X^*} + c_1)(2\sigma_{XX^*} + c_2)}{(\mu_X^2 + \mu_{X^*}^2 + c_1)(\sigma_X^2 + \sigma_{X^*}^2 + c_2)}. \tag{43}$$

where X and X^* are the front slices of tensors $\mathcal{X}$ and $\mathcal{X}^*$. Generally, we take the average of SSIM as the final SSIM value. Here, $c_1 = 2.55^2$ and $c_2 = 7.65^2$. μ_X and μ_{X^*} are the average values of X and X^*. σ_{XX^*} is the covariance matrix between X and X^*. σ_X^2 and $\sigma_{X^*}^2$ are variance of X and X^*. The higher the value of the SSIM, the better the algorithm performance.

4.2. Experimental Results and Analysis

We first analyze the computation time of the above methods, as shown in Figure 3. The abscissa represents resolution size, which are $64 \times 64 \times 3$, $128 \times 128 \times 3$, $256 \times 256 \times 3$, $516 \times 516 \times 3$, and $1024 \times 1024 \times 3$, respectively. The ordinate uses logarithmic scale to better reflect the difference of running time. It is easy to find that the proposed new model has more advantages in operation efficiency regardless of size. However, the computation cost of SPCQV and SPCTV is more expensive, since they involve PARAFAC/Polyadic Decomposition (PD) and estimation for the appropriate number of components in the smooth PD model.

Next, we test the performance of the above methods with an image of size $256 \times 256 \times 3$. We randomly remove 10% of elements and 50% of the ingredients, respectively, and add six kinds of noise interference into the observation area to form the damaged tensor data. The six kinds of noise interference, respectively, are: $N(0, 10)$ Gaussian noise, $N(0, 30)$ Gaussian noise, $N(0, 50)$ Gaussian noise, Poisson noise, salt and pepper noise, and speckle noise. We directly use the symbol "TNN" to represent the proposed model in Equation (40).

In the experiment, we evaluate the performance of the proposed model with $p = -1/2$ and $1/2$, TNN ($p = 1$), LRTV [1], SPCQV [29] and SPCTV [29]. The main reason for choosing $p = 1/2$ and $-1/2$ as representatives is the experimentally good performance of the proposed model in this case. In addition, the main reason for comparison TNN is to better illustrate the effect of low rank.

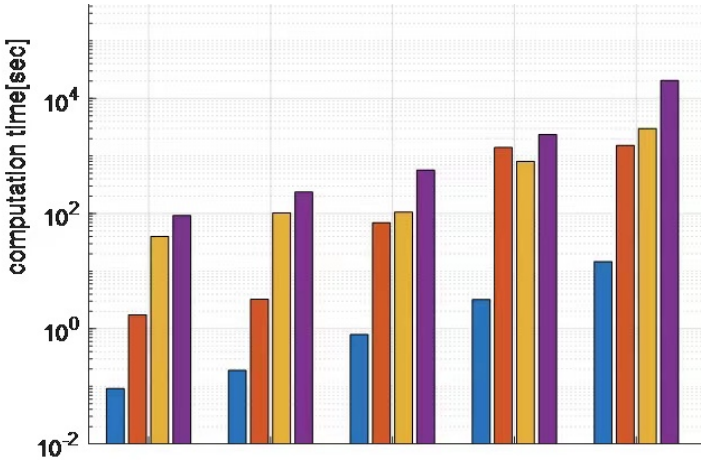


Figure 3. Comparison of computing time based on different methods, where "blue", "orange", "yellow", and "purple" refer, respectively, to the proposed model, LRTV [1], SPCTV [29], and SPCQV [29].

For the LRTV model, we use the parameter range suggested in reference [1]. w is set to $[0.5, 0.5, 0]$ and $\gamma = 0.05$. For SPCQV [29] and SPCTV [29], we also adopt the same optimal parameters. We set $\mu = 0.05$, $\beta = 10$ and choose α in the range $\{0.001, 0.01, 0.1, 1\}$. In fact, the experimental results are the best in this parameter range.

Here, we display the repairing results of two test images in the experiments. First, we randomly remove 30% of the 'House' voxels and add $N(0, 10)$ Gaussian noise to other areas. Figure 4 shows the intuitive experimental results from five methods. We selectively boost features of Lena's face, where the nostril integrity and cheek edge are shown in Figure 4. Compared with SPCQV [29], SPCTV [29], and LRTV [1], the completion results from the proposed approach are more complete and smooth (shown in the second line of Figure 4). Obviously, the proposed regularization terms can denoise and keep the original structure as far as possible from the overall and local point of view.

The first image located in the first line of Figure 5 is a damaged color image with a 50% missing rate and Poisson noise. "Original" represents the original image. There are obvious ceramic tile texture and clear edge lines in the roof. Overall, our method with $p = -1/2$ has the best performance. The results of SPCQV [29] and SPCTV [29] lost texture feature, while LRTV [1] and the methods based on TNN and $p = 1/2$ have a smooth transition.



Figure 4. Comparison of damaged image restoration under the 30% missing rate and Gaussian noise $N(0, 10)$.

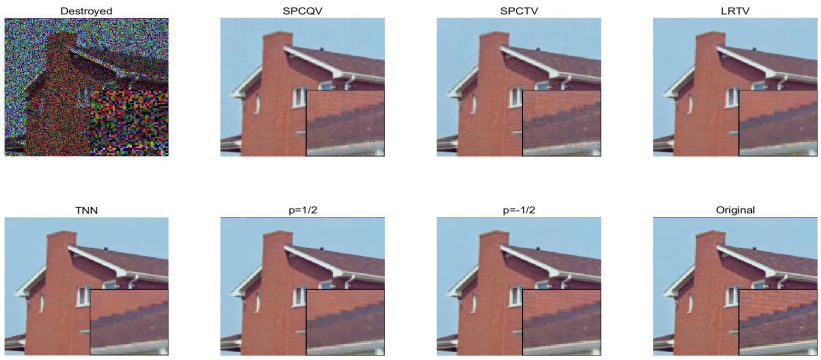


Figure 5. Comparison of damaged image restoration under the 50% missing rate and Poisson noise.

In this section, we report the comparison results of PSNR and SSIM of different models when the miss rate is 10% to 50% in Tables 1–4. These tables all contain six kinds of noise conditions. We use red to mark the optimal results between different models, which show that the new model has great potentiality in denoising and completion. For instance, when the test images miss 50% elements and add larger variance Gaussian noise, the performance of $p = -1/2$ model is better than other methods.

Numerically we can directly find that the difference between different p values of our model is small, but much larger than that of TNN-based models.This is consistent with the functional properties of p-TNN, which can discard some low singular values generated by noise and characterize the low rank of the image within a certain range of parameters.

Table 1. Comparisons of PSNR for images with 10% missing elements, where red is the best result.

	Miss Ratio = 10%											
	N(0,10)						**N(0,30)**					
	SPCQV [29]	**SPCTV [29]**	**LRTV [1]**	**TNN**	$p = \frac{1}{2}$	$p = -\frac{1}{2}$	**SPCQV [29]**	**SPCTV [29]**	**LRTV [1]**	**TNN**	$p = \frac{1}{2}$	$p = -\frac{1}{2}$
Airplane	35.61	35.54	35.97	37.39	38.57	38.59	32.65	32.61	33.62	34.25	34.75	34.71
Barbara	35.91	35.74	35.80	36.44	37.97	37.84	32.84	32.72	33.37	33.67	34.47	34.20
House	35.77	35.63	37.93	38.27	38.62	38.66	32.76	32.75	34.68	34.67	34.85	34.84
Lena	36.04	36.02	37.67	38.55	39.38	39.62	32.96	32.93	34.66	34.73	35.16	35.11
Monarch	35.98	35.71	36.07	37.36	39.51	39.73	32.79	32.61	33.58	34.14	34.96	34.95
Pepper	35.15	34.63	35.46	36.46	36.88	36.91	32.44	32.03	33.26	33.73	34.02	33.99
Boat	33.32	33.19	32.11	32.75	34.19	34.22	31.10	31.02	30.63	31.18	32.11	32.03
Giant	34.26	33.90	33.66	34.35	35.96	36.17	31.80	31.62	31.76	32.33	33.28	33.31
	N(0,50)						Possion					
Airplane	30.98	30.99	32.04	32.17	32.48	32.44	38.64	38.43	37.22	39.06	40.79	40.82
Barbara	31.00	30.90	31.81	31.83	32.30	32.12	38.96	38.66	36.91	37.24	39.35	39.61
House	31.07	31.05	32.60	32.34	32.55	32.52	38.39	38.18	39.61	39.46	39.85	39.87
Lena	31.17	31.13	32.66	32.50	32.73	32.64	39.50	39.33	38.88	39.74	41.19	41.17
Monarch	30.90	30.75	31.68	31.87	32.45	32.41	38.86	38.38	36.32	37.54	40.70	41.07
Pepper	30.72	30.40	31.72	31.89	32.02	31.99	35.26	33.34	35.29	33.64	34.54	36.47
Boat	29.98	29.87	30.01	30.30	30.92	30.79	34.59	34.49	32.44	33.21	34.86	35.11
Giant	30.54	30.25	30.84	31.14	31.72	31.71	36.03	35.54	34.39	35.13	37.18	37.76

Table 1. *Cont.*

	Miss Ratio = 10%											
	N(0,10)						N(0,30)					
	SPCQV [29]	**SPCTV [29]**	**LRTV [1]**	**TNN**	$p=\frac{1}{2}$	$p=-\frac{1}{2}$	**SPCQV [29]**	**SPCTV [29]**	**LRTV [1]**	**TNN**	$p=\frac{1}{2}$	$p=-\frac{1}{2}$
	Salt & Pepper						Speck					
Airplane	38.59	36.92	36.92	39.03	40.81	40.91	38.63	38.57	37.39	39.07	40.76	40.66
Barbara	39.03	38.69	36.88	37.43	39.39	39.62	38.87	38.56	36.69	37.29	39.24	39.45
House	38.24	38.07	39.45	39.53	39.86	39.90	38.20	38.06	39.26	39.28	39.75	39.73
Lena	39.67	39.19	38.98	39.75	41.23	41.22	39.85	39.46	39.10	39.96	41.31	41.25
Monarch	39.00	38.33	36.49	37.83	40.58	40.90	38.91	38.39	36.23	37.57	40.53	40.95
Pepper	34.81	33.27	35.35	33.65	34.44	36.44	35.29	34.08	35.33	33.70	34.56	36.44
Boat	34.34	34.25	32.19	33.02	34.72	35.05	34.68	34.51	32.26	32.98	34.93	35.20
Giant	35.84	35.58	34.21	35.11	37.35	37.98	35.89	35.59	34.16	34.90	37.34	37.97

Table 2. Comparisons of SSIM for images with 10% missing elements, where red is the best result.

	Miss Ratio = 10%											
	N(0,10)						N(0,30)					
	SPCQV [29]	**SPCTV [29]**	**LRTV [1]**	**TNN**	$p=\frac{1}{2}$	$p=-\frac{1}{2}$	**SPCQV [29]**	**SPCTV [29]**	**LRTV [1]**	**TNN**	$p=\frac{1}{2}$	$p=-\frac{1}{2}$
Airplane	0.9254	0.9207	0.9557	0.9617	0.9637	0.9627	0.8386	0.8356	0.8928	0.9038	0.9059	0.9044
Barbara	0.9538	0.9513	0.9681	0.9719	0.9743	0.9745	0.8989	0.8968	0.9299	0.9384	0.9403	0.9391
House	0.9159	0.9129	0.9479	0.9516	0.9529	0.9526	0.8215	0.8201	0.8796	0.8853	0.8867	0.8857
Lena	0.9312	0.9278	0.9624	0.9674	0.9692	0.9691	0.8501	0.8474	0.9050	0.9122	0.9138	0.9125
Monarch	0.9388	0.9350	0.9762	0.9825	0.9843	0.9834	0.8614	0.8584	0.9199	0.9319	0.9335	0.9324
Pepper	0.9283	0.9179	0.9426	0.9453	0.9458	0.9456	0.8532	0.8434	0.8917	0.8946	0.8952	0.8948
Boat	0.9449	0.9413	0.9539	0.9569	0.9593	0.9590	0.8844	0.8816	0.9110	0.9209	0.9233	0.9217
Giant	0.9555	0.9515	0.9678	0.9739	0.9771	0.9773	0.9094	0.9062	0.9351	0.9489	0.9518	0.9500
	N(0,50)						Possion					
Airplane	0.7778	0.7753	0.8347	0.8413	0.8438	0.8418	0.9821	0.9765	0.9676	0.9645	0.9763	0.9779
Barbara	0.8538	0.8516	0.8897	0.8965	0.8985	0.8969	0.9882	0.9852	0.9776	0.9746	0.9845	0.9854
House	0.7511	0.7496	0.8127	0.8117	0.8138	0.8132	0.9770	0.9739	0.9597	0.9565	0.9668	0.9694
Lena	0.7888	0.7866	0.8474	0.8501	0.8519	0.8505	0.9837	0.9795	0.9725	0.9694	0.9811	0.9818
Monarch	0.8035	0.8005	0.8632	0.8717	0.8737	0.8722	0.9904	0.9856	0.9868	0.9853	0.9905	0.9892
Pepper	0.7952	0.7858	0.8411	0.8407	0.8416	0.8409	0.9650	0.9478	0.9492	0.9450	0.9468	0.9533
Boat	0.8393	0.8365	0.8710	0.8803	0.8827	0.8809	0.9826	0.9787	0.9665	0.9631	0.9730	0.9738
Giant	0.8722	0.8682	0.9023	0.9171	0.9197	0.9177	0.9859	0.9818	0.9775	0.9774	0.9860	0.9858
	Salt & Pepper						Speck					
Airplane	0.9823	0.9678	0.9678	0.9646	0.9763	0.9779	0.9823	0.9766	0.9676	0.9644	0.9762	0.9779
Barbara	0.9883	0.9854	0.9775	0.9746	0.9845	0.9853	0.9881	0.9851	0.9772	0.9745	0.9844	0.9852
House	0.9768	0.9732	0.9592	0.9562	0.9666	0.9693	0.9770	0.9739	0.9590	0.9559	0.9666	0.9693
Lena	0.9839	0.9789	0.9727	0.9694	0.9813	0.9819	0.9839	0.9799	0.9729	0.9695	0.9812	0.9818
Monarch	0.9903	0.9858	0.9867	0.9854	0.9905	0.9892	0.9906	0.9856	0.9865	0.9853	0.9905	0.9893
Pepper	0.9643	0.9487	0.9492	0.9448	0.9464	0.9526	0.9652	0.9500	0.9491	0.9450	0.9468	0.9531
Boat	0.9825	0.9782	0.9663	0.9630	0.9732	0.9739	0.9828	0.9784	0.9666	0.9631	0.9733	0.9741
Giant	0.9855	0.9816	0.9772	0.9771	0.9862	0.9860	0.9853	0.9817	0.9772	0.9770	0.9860	0.9858

Table 3. Comparisons of PSNR for images with 50% missing elements, where red is the best result.

	Miss Ratio = 50%											
	N(0,10)						**N(0,30)**					
	SPCQV [29]	**SPCTV [29]**	**LRTV [1]**	**TNN**	$p = \frac{1}{2}$	$p = -\frac{1}{2}$	**SPCQV [29]**	**SPCTV [29]**	**LRTV [1]**	**TNN**	$p = \frac{1}{2}$	$p = -\frac{1}{2}$
Airplane	30.54	30.38	29.17	30.80	31.89	32.23	30.09	29.90	28.85	30.37	31.26	31.47
Barbara	30.39	29.65	28.54	29.24	30.10	30.95	29.69	28.92	28.22	28.96	29.64	30.15
House	30.96	30.54	32.40	32.66	33.39	33.86	30.65	30.33	31.58	31.86	32.59	32.89
Lena	31.63	31.24	31.69	32.56	33.22	33.68	31.04	30.52	31.07	31.79	32.34	32.56
Monarch	29.87	28.58	27.06	27.52	29.59	30.45	29.07	27.70	26.49	27.02	28.87	29.47
Pepper	30.06	28.76	29.00	29.36	30.07	30.42	29.35	28.07	28.59	28.92	29.49	29.62
Boat	25.97	25.35	24.25	24.44	25.56	26.03	25.78	25.13	24.27	24.37	25.37	25.83
Giant	27.23	26.39	25.49	25.59	27.00	27.92	26.79	25.97	25.21	25.29	26.61	27.33
	N(0,50)						Possion					
	SPCQV	SPCTV	LRTV	TNN	$p = \frac{1}{2}$	$p = -\frac{1}{2}$	SPCQV	SPCTV	LRTV	TNN	$p = \frac{1}{2}$	$p = -\frac{1}{2}$
Airplane	29.50	29.32	28.46	29.66	30.64	30.68	30.83	30.55	29.24	30.92	32.13	32.69
Barbara	28.98	28.19	27.86	28.38	28.98	29.34	30.76	30.01	28.83	29.56	30.44	31.43
House	30.14	29.76	30.79	30.97	31.53	31.71	31.10	30.87	32.37	32.69	33.49	33.98
Lena	30.37	29.89	30.53	31.15	31.56	31.67	32.15	31.73	31.94	32.73	33.46	34.25
Monarch	28.64	27.37	26.42	26.84	28.56	28.97	30.11	28.84	26.91	27.51	29.74	30.73
Pepper	28.63	27.45	28.07	28.42	29.01	29.05	29.49	27.82	28.59	27.28	27.77	29.15
Boat	25.36	24.79	24.06	24.29	25.14	25.53	26.16	25.52	24.30	24.40	25.57	26.12
Giant	26.41	25.52	24.98	25.03	26.26	26.90	27.36	26.61	25.51	25.59	27.10	27.97
	Salt & Pepper						Speck					
	SPCQV	SPCTV	LRTV	TNN	$p = \frac{1}{2}$	$p = -\frac{1}{2}$	SPCQV	SPCTV	LRTV	TNN	$p = \frac{1}{2}$	$p = -\frac{1}{2}$
Airplane	30.95	30.67	29.27	31.08	32.25	32.67	30.80	30.57	29.25	30.90	32.34	32.84
Barbara	30.85	30.07	28.87	29.40	30.34	31.30	30.69	29.97	28.81	29.41	30.26	31.17
House	31.00	30.75	32.42	32.65	33.51	34.05	30.95	30.72	32.43	32.50	33.34	33.83
Lena	32.12	31.62	31.77	32.63	33.34	34.14	32.00	31.50	31.73	32.66	33.26	34.07
Monarch	30.29	29.00	27.26	27.82	29.97	31.01	30.17	28.86	27.02	27.55	29.80	30.76
Pepper	29.79	28.13	28.60	27.45	27.98	29.29	29.72	27.96	28.39	27.19	27.77	29.10
Boat	26.17	25.56	24.46	24.47	25.68	26.24	26.29	25.61	24.54	24.64	25.70	26.29
Giant	27.41	26.60	25.56	25.49	27.11	28.02	27.51	26.76	25.58	25.69	27.27	28.17

Table 4. Comparisons of SSIM for images with 50% missing elements, where red is the best result.

	Miss Ratio = 50%											
	N(0,10)						**N(0,30)**					
	SPCQV [29]	**SPCTV [29]**	**LRTV [1]**	**TNN**	$p = \frac{1}{2}$	$p = -\frac{1}{2}$	**SPCQV [29]**	**SPCTV [29]**	**LRTV [1]**	**TNN**	$p = \frac{1}{2}$	$p = -\frac{1}{2}$
Airplane	0.8710	0.8486	0.8861	0.9001	0.9090	0.9096	0.8215	0.8015	0.8556	0.8787	0.8862	0.8845
Barbara	0.9076	0.8854	0.8917	0.9056	0.9165	0.9223	0.8732	0.8506	0.8736	0.8935	0.9017	0.9025
House	0.8609	0.8483	0.8882	0.8930	0.8983	0.9021	0.8114	0.7989	0.8559	0.8667	0.8717	0.8722
Lena	0.8892	0.8681	0.9098	0.9196	0.9262	0.9302	0.8443	0.8220	0.8808	0.8977	0.9033	0.9031
Monarch	0.9126	0.8781	0.9226	0.9344	0.9440	0.9442	0.8619	0.8278	0.8937	0.9153	0.9238	0.9210
Pepper	0.8633	0.8139	0.8716	0.8739	0.8772	0.8794	0.8176	0.7690	0.8471	0.8542	0.8568	0.8574
Boat	0.8605	0.8289	0.8443	0.8562	0.8733	0.8749	0.8234	0.7934	0.8240	0.8421	0.8546	0.8527
Giant	0.8871	0.8567	0.8638	0.8794	0.9014	0.9082	0.8541	0.8270	0.8448	0.8673	0.8823	0.8851

Table 4. *Cont.*

	Miss Ratio = 10%											
	N(0,10)						N(0,30)					
	SPCQV [29]	SPCTV [29]	LRTV [1]	TNN	$p=\frac{1}{2}$	$p=-\frac{1}{2}$	SPCQV [29]	SPCTV [29]	LRTV [1]	TNN	$p=\frac{1}{2}$	$p=-\frac{1}{2}$
	N(0,50)						Possion					
Airplane	0.7789	0.7603	0.8189	0.8421	0.8500	0.8477	0.9026	0.8773	0.8899	0.8985	0.9170	0.9245
Barbara	0.8421	0.8182	0.8496	0.8709	0.8792	0.8788	0.9263	0.9043	0.8986	0.9080	0.9249	0.9338
House	0.7661	0.7528	0.8148	0.8256	0.8302	0.8296	0.8911	0.8740	0.8857	0.8866	0.9040	0.9121
Lena	0.8020	0.7784	0.8450	0.8629	0.8679	0.8665	0.9172	0.8954	0.9134	0.9168	0.9338	0.9411
Monarch	0.8203	0.7865	0.8605	0.8835	0.8922	0.8887	0.9409	0.9043	0.9254	0.9329	0.9480	0.9529
Pepper	0.7760	0.7277	0.8166	0.8255	0.8265	0.8264	0.8777	0.8240	0.8660	0.8546	0.8585	0.8674
Boat	0.7906	0.7637	0.7996	0.8201	0.8317	0.8292	0.8839	0.8511	0.8508	0.8578	0.8823	0.8870
Giant	0.8299	0.8000	0.8248	0.8504	0.8639	0.8630	0.9039	0.8739	0.8677	0.8799	0.9085	0.9172
	Salt & Pepper						Speck					
Airplane	0.9024	0.8774	0.8881	0.8967	0.9171	0.9234	0.9021	0.8760	0.8882	0.8970	0.9167	0.9239
Barbara	0.9271	0.9060	0.8986	0.9071	0.9248	0.9333	0.9254	0.9039	0.8972	0.9058	0.9232	0.9319
House	0.8886	0.8730	0.8851	0.8857	0.9028	0.9113	0.8859	0.8730	0.8845	0.8850	0.9025	0.9108
Lena	0.9170	0.8927	0.9124	0.9158	0.9331	0.9401	0.9161	0.8933	0.9115	0.9152	0.9320	0.9399
Monarch	0.9417	0.9068	0.9268	0.9347	0.9501	0.9546	0.9417	0.9063	0.9259	0.9335	0.9496	0.9540
Pepper	0.8805	0.8263	0.8657	0.8552	0.8586	0.8667	0.8817	0.8256	0.8660	0.8537	0.8579	0.8670
Boat	0.8835	0.8519	0.8498	0.8564	0.8817	0.8865	0.8839	0.8495	0.8524	0.8593	0.8825	0.8877
Giant	0.9054	0.8738	0.8678	0.8799	0.9088	0.9177	0.9045	0.8747	0.8686	0.8806	0.9098	0.9187

5. Conclusions

In this paper, we propose the tensor relative total variation (TRTV) method, which integrates the local and global image information. Based on TRTV, we present a new tensor completion and denoising model, including tensor p-shrinkage nuclear norm minimization with a noise inequality constraint. Furthermore, we develop an ADMM-based algorithm to solve the proposed model. The experimental results show that the resulting model has great potentiality in denoising and completion.

Author Contributions: Conceptualization, Y.B. and J.P.; methodology, M.L.; software, Y.B.; validation, J.P. and M.L.; formal analysis, Y.B.; investigation, Y.B.; resources, Y.B.; data curation, Y.B.; writing—original draft preparation, Y.B.; writing—review and editing, J.P. and M.L.; visualization, Y.B.; supervision, J.P.; project administration, J.P. and M.L.; funding acquisition, J.P. and M.L. All authors have read and agreed to the published version of the manuscript.

Funding: This work was supported in part by the National Nature Science Foundation of China (62072312,62071303, 61972264) and in part by the Shenzhen Basis Research Project (JCYJ20210324094009026, JCYJ20200109105832261).

Institutional Review Board Statement: Not applicable.

Informed Consent Statement: Not applicable.

Data Availability Statement: The data presented in this study are available on request from the corresponding author.

Conflicts of Interest: There is no conflict of interest.

References

1. Yokota, T.; Hontani, H. Simultaneous tensor completion and denoising by noise inequality constrained convex optimization. *IEEE Access* **2019**, *7*, 15669–15682. [CrossRef]
2. Geng, S.-M.; Zhou, W. Exact matrix completion via convex optimization. *IEEE Access* **2009**, *6*, 717–772.
3. Srebro, N.; Shraibman, A. Rank, trace-norm and max-norm. In Proceedings of the Learning Theory: 18th Annual Conference on Learning Theory, COLT 2005, Bertinoro, Italy, 27–30 June 2005; pp. 545–560.

4. Hu, Y.; Zhang, D.; Ye, J.; Li, X.; He, X. Fast and accurate matrix completion via truncated nuclear norm regularization. *IEEE Trans. Pattern Anal. Mach. Intell.* **2012**, *35*, 2117–2130. [CrossRef]
5. Chen, Y.; Wang, S.; Peng, C.; Hua, Z.; Zhou, Y. Generalized nonconvex low-rank tensor approximation for multi-view subspace clustering.*IEEE Trans. Image Process.* **2021**, *30*, 4022–4035. [CrossRef]
6. Geng, X.; Smith-Miles, K.; Zhou, Z.-H.; Wang, L. Face image modeling by multilinear subspace analysis with missing valuesn. In Proceedings of the 17th ACM international conference on Multimedia, Vancouver, BC, Canada, 19–24 October 2009; pp. 629–632.
7. Liu, J.; Musialski, P.; Wonka, P.; Ye, J. Tensor completion for estimating missing values in visual data. *IEEE Trans. Pattern Anal. Mach. Intell.* **2012**, *35*, 208–220. [CrossRef]
8. Chen, Y.-L.; Hsu, C.-T.; Liao, H.-Y.M. Simultaneous tensor decomposition and completion using factor priors. *IEEE Trans. Pattern Anal. Mach. Intell.* **2013**, *36*, 577–591. [CrossRef]
9. Kruskal, J.B. Rank, decomposition, and uniqueness for 3-way and N-way arrays. *Multiway Data Anal.* **1989**, 7–18.
10. Fridtjov, I. *Tensor Analysis*; Springer: Berlin, Germany, 2019.
11. Itskov, M. *Tensor Algebra and Tensor Analysis for Engineers: With Applications to Continuum Mechanics*; Springer: Berlin, Germany, 2013.
12. Kolda, T.G.; Bader, B.W. Tensor Decompositions and Applications. *SIAM Rev.* **2009**, *51*, 455–500. [CrossRef]
13. Zhang, Z.; Ely, G.; Aeron, S.; Hao, N.; Kilmer, M. Novel methods for multilinear data completion and de-noising based on tensor-SVD. In Proceedings of the IEEE Conference on Computer Vision and Pattern Recognition, Columbus, OH, USA, 23–28 June 2014; pp. 3842–3849.
14. Zhang, Z.; Aeron, S. Exact tensor completion using t-SVD.*IEEE Trans. Signal Process.* **2016**, *65*, 1511–1526. [CrossRef]
15. Friedland, S.; Lim, L.-H. Nuclear norm of higher-order tensors. *Math. Comput.* **2018**, *87*, 1255–1281. [CrossRef]
16. Lu, C.; Zhou, P. Exact recovery of tensor robust principal component analysis under linear transforms. *arXiv* **2019**, arXiv:1907.08288.
17. Xu, W.-H.; Zhao, X.-L.; Ji, T.-Y.; Miao, J.-Q.; Ma, T.-H.; Wang, S.; Huang, T.-Z. Laplace function based nonconvex surrogate for low-rank tensor completion. *Signal Process. Image Commun.* **2019**, *73*, 62–69. [CrossRef]
18. Foucart, S. Concave Mirsky inequality and low-rank recovery. *SIAM J. Matrix Anal. Appl.* **2018**, *39*, 99–103. [CrossRef]
19. Kilmer, M.E.; Braman, K.; Hao, N.; Hoover, R.C. Third-order tensors as operators on matrices: A theoretical and computational framework with applications in imaging. *SIAM J. Matrix Anal. Appl.* **2013**, *34*, 148–172. [CrossRef]
20. Li, M.; Yang, Y.; Xu, L.; Xu, C.; Sun, X. Salient Object Detection Based on Unified Convex Surrogate for Non-Convex Schatten-*p* Norm. *IEEE Access* **2020**, *8*, 20171–20180. [CrossRef]
21. Nie, F.; Huang, H.; Ding, C. Low-rank matrix recovery via efficient schatten p-norm minimization. In Proceedings of the AAAI Conference on Artificial Intelligence, Phoenix, AZ, USA, 12–17 February 2016; pp. 655–661.
22. Xu, C.; Lin, Z.; Zha, H. A unified convex surrogate for the Schatten-p norm. In Proceedings of the AAAI Conference on Artificial Intelligence, San Francisco, CA, USA, 4–9 February 2017.
23. Zhang, M.; Huang, Z.-H.; Zhang, Y. Restricted *p*-isometry properties of nonconvex matrix recovery. *IEEE Trans. Inf. Theory* **2013**, *59*, 4316–4323. [CrossRef]
24. Yang, C.; Wang, W.; Feng, X.; Liu, X. Weighted-l1-method-noise regularization for image deblurring. *Signal Process.* **2019**, *157*, 14–24. [CrossRef]
25. Xu, S.; Zhang, J.; Zhang, C. Hyperspectral image denoising by low-rank models with hyper-Laplacian total variation prior. *Signal Process.* **2022**, *108733*, 1–10.
26. Zeng, H.; Xie, X.; Ning, J. Hyperspectral image denoising via global spatial-spectral total variation regularized nonconvex local low-rank tensor approximation. *Signal Process.* **2021**, *107805*, 1–16. [CrossRef]
27. Liu, C.; Shan, H.; Chen, C. Tensor p-shrinkage nuclear norm for low-rank tensor completion.*Neurocomputing* **2020**, *387*, 255–267. [CrossRef]
28. Yokota, T.; Hontani, H. Simultaneous visual data completion and denoising based on tensor rank and total variation minimization and its primal-dual splitting algorithm. In Proceedings of the IEEE Conference on Computer Vision and Pattern Recognition, Honolulu, HI, USA, 21–26 July 2017; pp. 3732–3740.
29. Yokota, T.; Zhao, Q.; Cichocki, A. Smooth PARAFAC decomposition for tensor completion. *IEEE Trans. Signal Process.* **2016**, *64*, 5423–5436. [CrossRef]
30. Kilmer, M.E.; Martin, C.D. Factorization strategies for third-order tensors. *Linear Algebra Its Appl.* **2011**, *435*, 641–658. [CrossRef]
31. Kernfeld, E.; Kilmer, M.; Aeron, S. Tensor–tensor products with invertible linear transforms. *Linear Algebra Its Appl.* **2015**, *485*, 545–570. [CrossRef]
32. Voronin, S.; Chartrand, R. A new generalized thresholding algorithm for inverse problems with sparsity constraints. In Proceedings of the 2013 IEEE International Conference on Acoustics, Speech and Signal Processing, Vancouver, BC, Canada, 26–31 May 2013; pp. 1636–1640.
33. He, W.; Zhang, H.; Zhang, L.; Shen, H. Total-variation-regularized low-rank matrix factorization for hyperspectral image restoration. *IEEE Trans. Geosci. Remote Sens.* **2017**, *54*, 178–188. [CrossRef]
34. Osher, S.; Burger, M.; Goldfarb, D.; Xu, J.; Yin, W. An iterative regularization method for total variation-based image restoration. *Multiscale Model. Simul.* **2005**, *4*, 460–489. [CrossRef]
35. Wu, Z.; Wang, Q.; Wu, Z.; Shen, Y. Total variation-regularized weighted nuclear norm minimization for hyperspectral image mixed denoising. *J. Electron. Imaging* **2016**, *25*, 13–37. [CrossRef]

36. Wang, Y.; Peng, J.; Zhao, Q.; Leung, Y.; Zhao, X.-L.; Meng, D. Hyperspectral image restoration via total variation regularized low-rank tensor decomposition. *IEEE J. Sel. Top. Appl. Earth Obs. Remote Sens.* **2017**, *11*, 1227–1243. [CrossRef]
37. Xu, L.; Yan, Q.; Xia, Y.; Jia, J. Structure extraction from texture via relative total variation. *ACM Trans. Graph. (TOG)* **2012**, *31*, 1–10. [CrossRef]

Disclaimer/Publisher's Note: The statements, opinions and data contained in all publications are solely those of the individual author(s) and contributor(s) and not of MDPI and/or the editor(s). MDPI and/or the editor(s) disclaim responsibility for any injury to people or property resulting from any ideas, methods, instructions or products referred to in the content.